This article has been accepted for publication in a future issue of this journal, but has not been fully edited. Content may change prior to final publication. Citation information: DOI 10.1109/JPHOT.2018.2856506, IEEE Photonics Journal

Analysis of Coupling Losses for All-fiber Integration of Subwavelength Core Hybrid Optical Fibers

Yucheng Ye[1], Limin Xiao[1,2,3*], Shaohua Dong[1] and Anna C. Peacock[4]

[1] Advanced Fiber Devices and Systems Group, Key Laboratory of Micro and Nano Photonic structures (MoE), Department of Optical Science and Engineering, School of Information Science and Technology, Fudan University, Shanghai 200433, China

[2] Key Laboratory for Information Science of Electromagnetic Waves (MoE), Fudan University, Shanghai 200433, China

[3] Shanghai Engineering Research Center of Ultra-Precision Optical Manufacturing, Fudan University, Shanghai 200433, China

[4] Optoelectronics Research Centre, University of Southampton, Southampton, SO17 1BJ, United Kingdom

*corresponding author: liminxiao@fudan.edu.cn

Abstract: Coupling losses for all-fiber integration of subwavelength core hybrid optical fibers have been first analyzed and optimized in detail. We have taken into account the effects of mode size, mode shape, effective refractive index, tapering beat length, interface and endface reflections on the coupling loss. By optimizing parameters such as the subwavelength core diameter, single mode condition and transition length, the coupling losses can be reduced. In addition, the influence of the core fabrication and misalignment tolerances have been explored. The results will benefit the all-fiber integration of hybrid optical fibers and their nano-engineering realization.

Index Terms: Coupling loss, fiber devices, subwavelength waveguide, all-fiber devices

1. Introduction

Subwavelength-scale optical waveguides and devices have attracted intense interest for their unique optical properties, enhanced optical functions, increased device miniaturization and integration. In planar waveguides various ultra-compact devices have been developed such as subwavelength photonic circuits [1, 2], plasmonics devices [3], on-chip nanotapers [4], and subwavelength gratings [5, 6], offering significant benefits for a wide range of applications. Low-loss coupling for planar silicon nanophotonic devices has been widely investigated, which is critical for practical applications [4, 7, 8]. Another type of subwavelength optical device is based on optical fibers. These fibers can have subwavelength core diameters over macroscopic length scales, spanning millimeter to kilometer ranges, to provide a specific link between their macroscopic and microscopic features. Thus these subwavelength fiber waveguides possess the advantages of subwavelength structures and long interaction length simultaneously.

The most distinguished subwavelength fiber waveguide examples are probably the micro/nano-fibers (MNFs) and the nonlinear photonic crystal fibers (PCFs). MNFs are air-clad optical fibers with glass core diameters on a micro/nano-scale [9]. They have many advantages such as excellent mechanical flexibilities, tight optical confinement, large fractional evanescent fields, abnormal waveguide dispersion and low power consumption, which makes them idea waveguides for optical micro-device fabrication, light manipulation and low-loss connection [9, 10]. Different applications based on MNFs have been developed such as micro-resonators [11-13], optical tweezers [14] and plasmonic nanowire coupling [10]. Another successful example is the highly nonlinear PCFs, which also have small micrometer sized-cores and high air-fraction microstructured claddings, and thus have been widely used in commercial supercontinuum generation and other nonlinear applications [15-19].

The material mainly used to fabricate MNFs and nonlinear PCFs is fused silica. However, inspired by the great success of these silica fiber waveguides, there has been recent interest in exploring other

This article has been accepted for publication in a future issue of this journal, but has not been fully edited. Content may change prior to final publication. Citation information: DOI 10.1109/JPHOT.2018.2856506, IEEE Photonics Journal

materials in the fiber geometry to broaden the light transmission windows and access new functionalities [18-20]. Recently, hybrid optical fibers (HOFs) [21, 22] that incorporate materials such as semiconductors [23, 24], soft-glasses [19], and nonlinear liquids [25-27] have been investigated intensely. These HOFs generally have a solid or microstructured silica cladding with the new material incorporated in the core, with the most common materials for each fiber type being silicon, chalcogenide glasses and carbon disulfide, respectively. The incorporation of these new materials can overcome some of the limitations of silica, with fruitful applications in areas such as mid-infrared power generation and delivery [18, 28], broadband supercontinuum generation [28, 29], Raman amplification [25], all-optical modulation [30], and ultrafast all-optical switches [31]. Because the refractive indices of core materials are much higher than that of the silica cladding, to maintain single mode, or even few mode operation, the HOF generally has a small core in the wavelength or subwavelength scale. This has advantages for nonlinear applications due to the reduced effective mode area, but presents significant challenges in terms of low loss fiber fabrication and coupling.

Precise fabrication is a key challenge for the small-core HOFs. With improved drawing techniques and advanced infiltration approaches, HOFs have been manufactured via a variety of methods such as high pressure chemical vapor deposition [32], molten core fiber drawing [24, 33], powder-in-tube drawing [34], aluminum rod-in-tube drawing [35], capillary force filling [36], and pressure-assisted melt-filling [37]. Different post-processing methods have also been proposed to improve their optical qualities [38, 39]. However, in general it is not easy to draw small core HOFs because of distinct differences in the melting temperatures and material incompatibility, and thus tapering techniques have been investigated to decrease the core diameter and improve the material properties in such fibers [38]. Although significant progress has been made in the fabrication and optimization of these HOFs, there is still room for improvement, especially for the semiconductor-core optical fibers where the propagation losses are relatively high compared with single crystal semiconductor planar waveguides [39].

The second major challenge for small-core HOF applications is all-fiber integration. It is crucial to achieve a low loss robust connection or splicing with standard single mode fibers (SMFs) to avoid bulky lens coupling. The high interface reflection of the HOF and the large mode mismatching are the main hurdles to obtaining low loss all-fiber connection, and the effects of fabrication tolerances and alignment error have not been fully considered. Several coupling experiments have been carried out on small core HOFs [25, 40, 41]. Coupling light into the HOF with a tapered subwavelength core, or nanospike as it has been termed, is a promising technique [18, 40, 41]. For example, free space coupling through a nanospike was used for a chalcogenide HOF with the core diameter of 0.183 μm to decrease the interface reflection and laser damage [40], resulting in a coupling loss of 2.2 dB. Using a similar method, the all-fiber coupling loss was around 4 dB between a SMF and a silicon HOF with a core diameter of 1.1 μm [41]. The coupling loss between a carbon disulfide HOF with a core diameter of 1.75 μm and a SMF was also found to be around 40% [25]. Clearly, in all these cases the connection losses between small core HOFs and standard SMFs were high and the fabrication tolerances were not discussed. Thus, progress in this area has been impeded by a lack of an optimized design, nanoengineering characterization and analysis.

In this paper, we have optimized the parameters of HOFs for low-loss integration of HOFs and SMFs using a subwavelength tapered core approach, and analyzed the effects of the fabrication tolerances and alignment errors in detail. The mode properties of various HOFs were characterized and the optimized parameters for mode matching between different types of HOFs and SMFs were investigated using a full-vector finite element method. Specifically, tolerances of the tapered core (or spike) diameter deviation, the lateral misalignment error, optimized tapered transition length and the specific interface reflection have been fully considered. Thus this work provides the optimized intervals of the key parameters, which could guide the HOF design and accelerate the progress of low loss all-fiber HOF integration.

2. Optimized Interface Coupling Loss

For the small core HOFs, two different approaches can be used to reduce the coupling loss between HOFs and conventional SMFs in principle, as shown in Fig. 1. One approach is to use a large taper (Fig.1(a)) to match the SMF, however, the high index core material and large core diameter will cause high interface reflection loss and multimode coupling loss. The other approach is to use a subwavelength tapered core structure, which can improve the mode matching, decrease the interface reflection and allow for efficient fundamental mode conversion at the joint. Thus we only consider the latter approach to

This article has been accepted for publication in a future issue of this journal, but has not been fully edited. Content may change prior to final publication. Citation information: DOI 10.1109/JPHOT.2018.2856506, IEEE Photonics Journal

optimize the coupling efficiency. The interface coupling loss between the SMF and the HOF nanospike is then calculated.

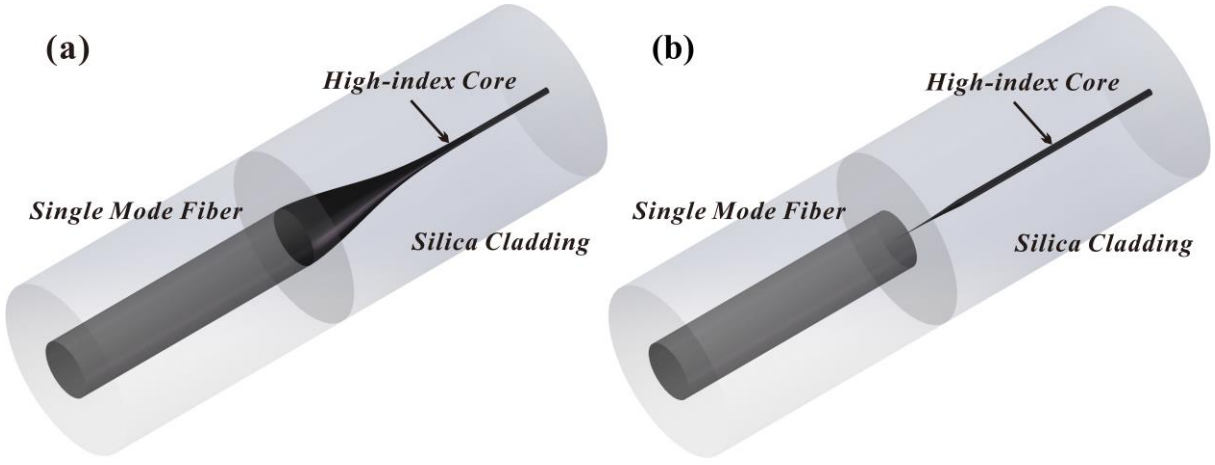

Fig. 1. Schematic diagrams of splicing between a SMF and a HOF using techniques of (a) large taper structure, and (b) subwavelength-core taper structure.

The interface coupling loss between a SMF and a tapered HOF nanospike shown in Fig. 1(b) can be calculated using a full vector method [42, 43], The equations are described in terms of the normalized vector electric field $\mathbf{E_i}$ and magnetic field $\mathbf{H_i}$ of the HE_{11} mode of the SMF, and the corresponding fields $\mathbf{E_t}$ and $\mathbf{H_t}$ of the subwavelength core HOF. The calculated modes are normalized to carry 1 W power,

$$\left\langle \mathbf{E_i} \middle| \mathbf{H_i} \right\rangle = \frac{1}{2}\mathrm{Re}\left(\int dA \left(\mathbf{E_i} \times \mathbf{H_i^*} \right) \cdot \hat{\mathbf{z}} \right) = 1, \tag{1}$$

$$\left\langle \mathbf{E_t} \middle| \mathbf{H_t} \right\rangle = \frac{1}{2}\mathrm{Re}\left(\int dA \left(\mathbf{E_t} \times \mathbf{H_t^*} \right) \cdot \hat{\mathbf{z}} \right) = 1, \tag{2}$$

where A is the cross-sectional area of the fiber. The field transmission (t) and reflection (r) coefficients can be expressed as

$$t = \frac{2\left\langle \mathbf{E_t} \middle| \mathbf{H_i} \right\rangle \left\langle \mathbf{E_i} \middle| \mathbf{H_t} \right\rangle}{\left\langle \mathbf{E_t} \middle| \mathbf{H_i} \right\rangle + \left\langle \mathbf{E_i} \middle| \mathbf{H_t} \right\rangle}, \tag{3}$$

$$r = \frac{\left\langle \mathbf{E_t} \middle| \mathbf{H_i} \right\rangle - \left\langle \mathbf{E_i} \middle| \mathbf{H_t} \right\rangle}{\left\langle \mathbf{E_t} \middle| \mathbf{H_i} \right\rangle + \left\langle \mathbf{E_i} \middle| \mathbf{H_t} \right\rangle}. \tag{4}$$

The power transmission (T), reflection (R), and coupling loss (L) are given by

$$T = t^2, \tag{5}$$

$$R = r^2, \tag{6}$$

$$L = -10\log(T). \tag{7}$$

This full-vector numerical method takes into account important factors such as the mode field diameter (MFD), mode shape and the Fresnel reflection between two fiber interfaces [42, 43]. All these factors are critical in determining the coupling loss. To verify our approach, we used this method to obtain the previous simulation results in Ref. [43].

Another approximate equation to calculate the coupling loss can be expressed as below [44, 45]:

$$L = -20\log\left(\frac{2\omega_1\omega_2}{\omega_1^2 + \omega_2^2} \right), \tag{8}$$

where ω_1 and ω_2 are the MFD of the SMF and the tapered HOF at the joint interface. This simple method is widely used to estimate the fiber coupling loss due to the mode field mismatch, but it neglects reflections losses and mode shapes. For a Gaussian-like mode, the MFD is the separation between the two points where the intensity of power is $1/e^2$ of the maximum power. Since the intensity distribution of the HOF at subwavelength scale is not a Gaussian-like shape, the MFD should be given by [46]:

This article has been accepted for publication in a future issue of this journal, but has not been fully edited. Content may change prior to final publication. Citation information: DOI 10.1109/JPHOT.2018.2856506, IEEE Photonics Journal

$$\omega = 2\sqrt{2}\left(\frac{\int\left|\mathbf{E}\times\mathbf{H}^*\right|_z r^2 d^2\mathbf{r}}{\int\left|\mathbf{E}\times\mathbf{H}^*\right|_z d^2\mathbf{r}}\right)^{\frac{1}{2}}. \tag{9}$$

The coupling losses and MFDs of different types of HOFs are then calculated using the full-vector method. Refractive indices of Si, As_2S_3 and CS_2 core materials at the wavelength of 1550 nm are 3.475, 2.437, and 1.588, respectively [47-49], and the refractive index of the silica cladding is 1.444. The core diameter of Corning SMF28 is 8.2 μm, the numerical aperture is 0.14 at telecoms waveguides, and the refractive index difference between core and cladding is 0.36%. The minimum coupling losses for the tapered HOF structures with Si, As_2S_3 and CS_2 core materials are calculated to be 0.32 dB, 0.32 dB, and 0.31 dB, corresponding to nanospike diameters of 0.18 μm, 0.24 μm, and 0.62 μm, respectively. The MFDs at these diameters were calculated to be 11.8 μm, 11.9 μm and 11.7 μm, with the mode field pattern shown in Fig 2 (b-d). The interface coupling losses as a function of the tapered HOF core diameters will be analyzed in more detail in part 4. It is not surprising that the minimum losses are not zero, which is mainly due to the difference in the mode shapes because the interface reflection is very low, as will be discussed in part 5. As we can see from Fig. 2(b-d), the mode profile of a circular core of the HOF is not circular because of the abrupt dielectric discontinuity of high index contrast waveguide.

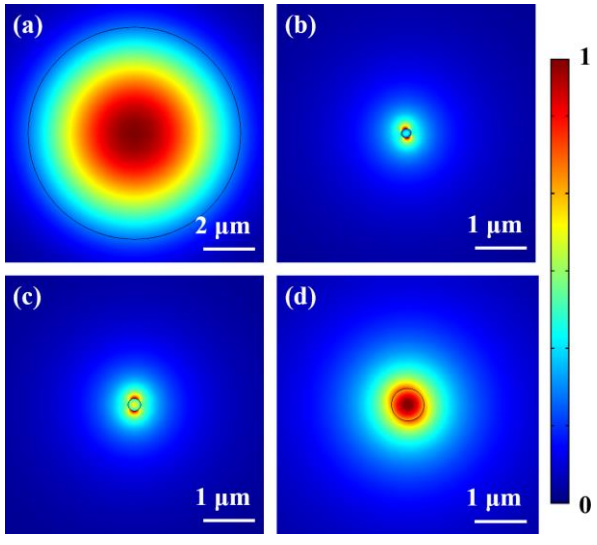

Fig. 2. The mode pattern of (a) SMF28. The mode patterns of the tapered HOFs under optimized conditions: (b) 0.18 μm Si core, (c) 0.24 μm As_2S_3 core, and (d) 0.62 μm CS_2 core fibers.

The boundary condition at a dielectric interface requires that the normal electrical displacement component should be continuous, thus making the normal electrical field discontinuous at the interface [50]. The y-polarized fundamental modes of the Si and CS_2 tapered HOFs, which match the MFD of a SMF, are illustrated in Fig.3(a, c). It can be noticed that, although the intensity reduces quickly inside the core, it increases abruptly in the cladding region, by the ratio of n^2_{core}/n^2_{clad} at the boundary. The discontinuity of the intensity profile along the Y axis is caused by the large discontinuity of the electrical field along the Y axis [49]. What's more, subwavelength core HOFs show azimuthal angle dependent profiles, i.e., the mode profiles in various azimuthal angles are different as shown in Fig. 3(b, d). Compared with a SMF28, where the mode profiles are identical in all azimuthal directions (Fig.2(c)), the mode profile of the subwavelength Si-core HOF is not continuous and the discontinuity is very different in various azimuthal directions. In the azimuthal angles of 0°, 30°, 60° and 90°, the intensity ratio of maximum power in the cladding and in the core are 2.36, 1.90, 1.13 and 0.96 respectively. For the CS_2-core HOF, the intensity ratio of the maximum power in the cladding and in the core are 0.84, 0.80 and 0.74 in the azimuthal angles of 0°, 30°, 60°. It should be mentioned that although the mode profile of the subwavelength-core HOF is azimuthal angle dependent, the coupling is polarization independent.

This article has been accepted for publication in a future issue of this journal, but has not been fully edited. Content may change prior to final publication. Citation information: DOI 10.1109/JPHOT.2018.2856506, IEEE Photonics Journal

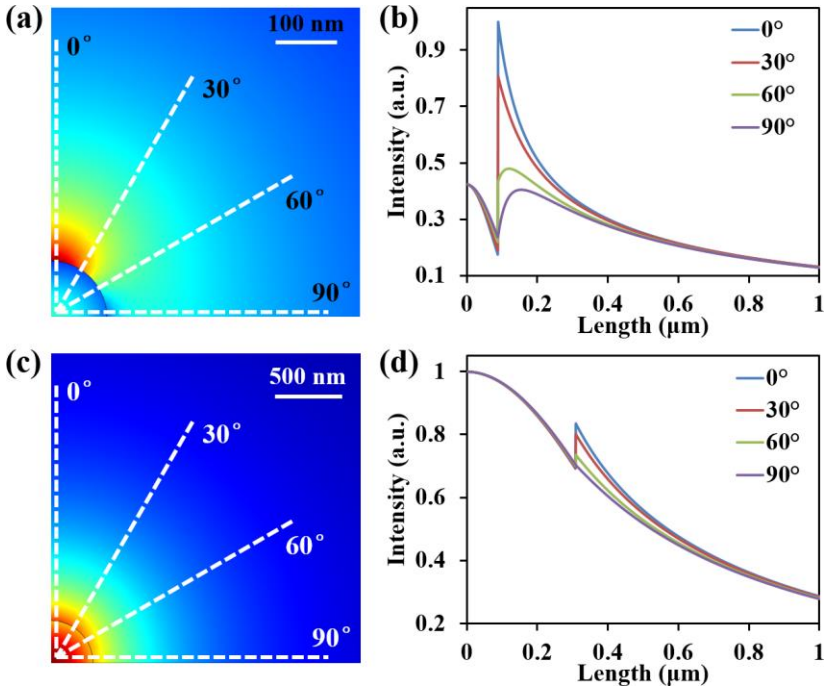

Fig. 3. The mode patterns (a) and normalized intensity profile of the y-polarized mode in different directions (b) for a 0.18 μm Si-core HOFs. (c) and (d) are for a 0.62 μm CS_2–core HOF

Actually the coupling loss is quite low considering the difference in the mode profiles. Besides the contribution of the similar MFDs, the fact that the effective mode indices between the subwavelength tapered core HOFs and SMFs are also similar, helps to keep the losses down. The same effective mode index is an important factor for efficient mode coupling in fiber couplers and mode converters. We noticed that the effective mode indices of the small-core HOFs decrease sharply with the decrease of the core diameter shown in Fig. 4, approaching the index of silica cladding when the core diameters are the optimized values.

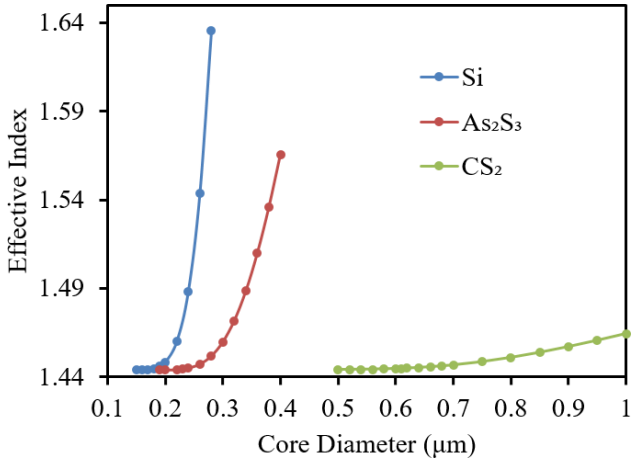

Fig. 4. The effective indices of the tapered HOFs as a function of the core diameters.

3. Taper Transition

Optimized nanospikes at the HOFs interfaces could provide an elegant coupling solution to SMFs. However, as a smooth transition from the tip of the nanospike to the untapered HOF core is also important for low-loss coupling, a suitable tapering transition is essential. Here we only consider the

This article has been accepted for publication in a future issue of this journal, but has not been fully edited. Content may change prior to final publication. Citation information: DOI 10.1109/JPHOT.2018.2856506, IEEE Photonics Journal

transition lengths for coupling to small core HOFs that support single mode guidance. To be a single mode fiber waveguide, the core diameter of the HOF can be calculated by Equation (10) [51]:

$$V = 2\pi \cdot \frac{D}{2\lambda_0} \cdot (n_{core}^2 - n_{cladding}^2)^{\frac{1}{2}} \le 2.405. \tag{10}$$

Thus a single-mode HOF should have a much smaller core diameter than that of the normal SMF because of large refractive index contrast between the core and the cladding. The larger the index contrast, the smaller the core size to maintain single mode guidance. The single-mode conditions for Si, As_2S_3, and CS_2 core HOFs at wavelength of 1550 nm are 0.37 μm, 0.60 μm, and 1.80 μm, respectively. So the single mode HOF has a very small core, and the corresponding MFD is also quite tiny. For example, the MFDs of single-mode HOFs with 0.37 μm Si, 0.60 μm As_2S_3 and 1.80 μm CS_2 cores are 0.42 μm, 0.68 μm, and 1.99 μm, respectively. To form a low loss transition, it is important to keep an adiabatic transition, thus the taper transition length should be much longer than the beat length (BL) [52]:

$$BL = \frac{2\pi}{\beta_1 - \beta_2}, \tag{11}$$

where β_1 and β_2 are propagation constants of fundamental mode in the HOF core and the cladding mode of the silica cladding, respectively. Fig.7 shows the beat length curve as a function of the core diameter at 1550 nm. The beat length increases slowly for large core diameters, but rises steeply for smaller core diameters in the deep subwavelength range. For example, the beat lengths of the above single-mode HOFs are 1.83 μm, 3.35 μm, and 20.7 μm, respectively. For the Si, As_2S_3 and CS_2 HOFs with nanospike tip dimensions of 0.18 μm, 0.24 μm, and 0.62 μm (as calculated in Section 2), the beat lengths are 2.12 mm, 1.42 mm, and 1.87 mm, respectively, so the transition length should be much larger than these values. For example, a smooth taper transition with the length of 5 mm could be used to achieve low loss transition for all these HOFs. This relatively long smooth taper can guarantee that light is well guided in the core, not coupled to the cladding modes. The results presented here offer a valuable reference for the fabrication of fiber-based coupling structures.

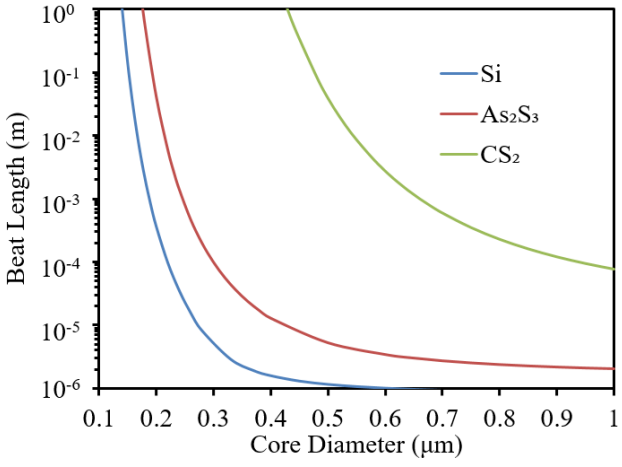

Fig. 5. The beat length as a function of the core diameter of the HOF

4. Core size and alignment errors

In practical fiber tapering and connection processes, it is inevitable that errors will occur in the core size of the tapered HOF nanospike region as well as the lateral alignment between the HOFs and SMFs. These errors will affect the coupling loss significantly and care should be taken when analyzing the loss tolerances and carrying out practical operation.

This article has been accepted for publication in a future issue of this journal, but has not been fully edited. Content may change prior to final publication. Citation information: DOI 10.1109/JPHOT.2018.2856506, IEEE Photonics Journal

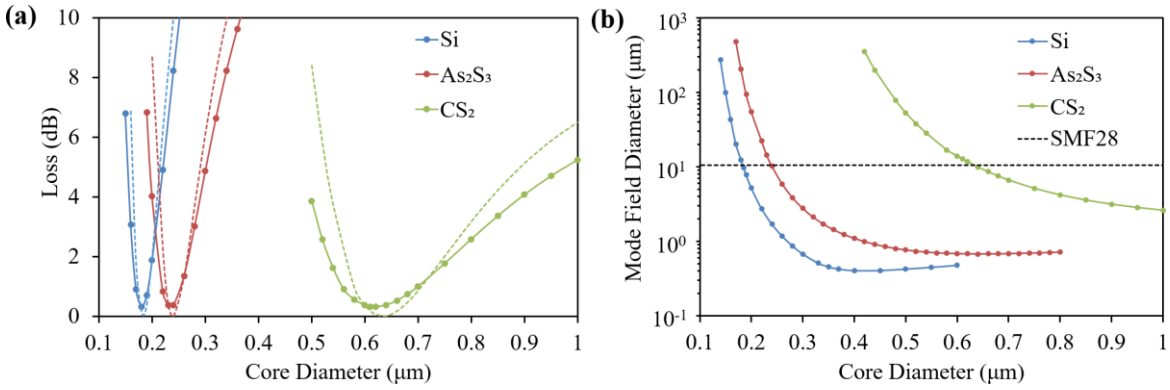

Fig. 6. (a) The coupling loss calculated by the accurate model of Eq. (7) (solid line) and approximate model in Eq. (8) (dashed line). (b) MFD of HOFs as a function of the core diameter.

Fig.6 (a) shows the interface coupling loss between a SMF28 and a HOF nanospike as a function of the core diameter. The coupling loss first decreases and then increases when reducing the core diameter. The solid line represents results for the full-vector model. For the Si, As_2S_3 and CS_2 core nanospike, the core diameters should be in the range of 0.185±0.025 μm, 0.245±0.035 μm and 0.67±0.16 μm, respectively, to achieve losses less than 3 dB, and in the range of 0.18±0.01 μm, 0.235±0.015 μm, and 0.63±0.07 μm to achieve losses less than 1dB. We note that the higher the core refractive index, the smaller the optimized nanospike core, as these smaller cores support a larger expanded mode to facilitate mode matching with the SMF28. It is also apparent that the nanospike ends with higher index core materials have relatively smaller tolerance ranges for low loss coupling. This could be explained by the MFD variation with the core size. We can observe from Fig.6 (b) that the MFD varies more rapidly when it is close to the MFD of SMF28 in the case of the larger core index. It is also demonstrated in the U-shaped curves (Fig. 6(a)), the higher index contrast HOF has a narrower U-shaped curve with the core diameter variation. So any small error in the fabrication will affect the coupling loss significantly when the HOF nanospike has a higher index contrast structure. For example, the Si-core HOF has a core size tolerance of only ±0.01 μm to achieve a loss below 1dB. On simply inspection of Fig. 6(a) it seems that the positive and negative errors in the minimum core size will cause the same loss if only the interface coupling is considered. However, we believe that the positive and negative tolerances will affect the coupling losses differently because the smaller core needs a longer taper length to achieve an adiabatic transition, especially for the core size in the subwavelength scale, which has a significantly increased beat length. As discussed in Section 3, the transition length of the taper is also critical for low loss coupling. For example, the beat lengths of Si-core nanospikes with core diameters of 0.17 μm and 0.19 μm are 6.6 mm and 0. 8 mm. It is obviously easier for the nanospike with a 0.19 μm sized core at the interface to achieve a low loss adiabatic transition, thus, in practice, a positive error will be preferred.

We also compared the accurate model and the approximate model in Fig. 6 (a). The dashed line represents the approximate MFD model. Although it is not as accurate as the full-vector model (solid lines), we find it can predict the optimized core diameter of the nanospike. The core diameters corresponding to the lowest coupling losses for Si, As_2S_3 and CS_2 are 0.185, 0.24, 0.64 μm respectively, which matches well with the full-vector model. However, the approximate model could not be used to calculate the core size tolerance intervals of the HOF nanospikes, especially for the liquid core HOF because of distinct difference between the precise model and approximate model.

This article has been accepted for publication in a future issue of this journal, but has not been fully edited. Content may change prior to final publication. Citation information: DOI 10.1109/JPHOT.2018.2856506, IEEE Photonics Journal

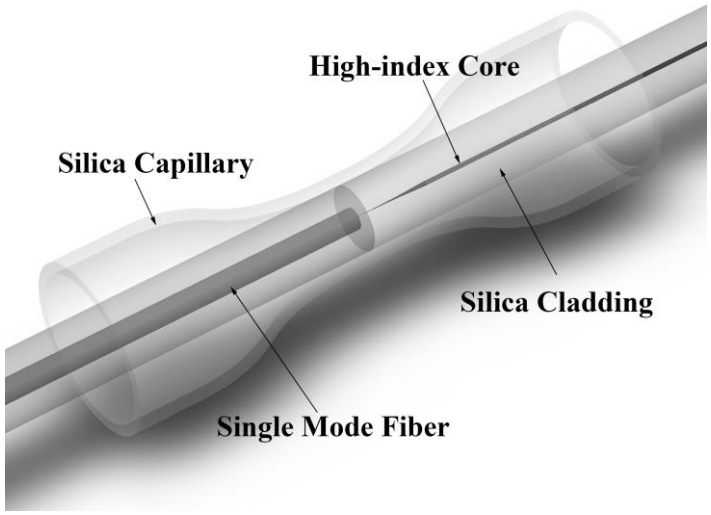

Fig. 7. Schematic diagram of mechanical splicing between a SMF and a HOF inside a tapered capillary.

Lateral alignment errors will naturally occur in the process of splicing or connecting fibers, and these have been fully studied for traditional SMFs [53]. However, the coupling losses to HOFs related to the lateral offset have not yet been investigated. HOFs generally possess two incompatible materials with distinctly different melting temperatures, it is therefore not easy to undertake low-loss fusion splicing, and mechanical splicing is an alternative approach to achieve a compact and robust connection. As shown in Fig.7, the two fibers could be aligned and mechanically spliced in a tapered silica capillary [54], and then assembly could be constructed using epoxy. This method has been utilized for all-fiber liquid-core HOFs. So the lateral alignment errors should be analyzed to identify fabrication and alignment accuracy.

Fig. 8 shows coupling losses for the three types of HOFs as a function of lateral alignment errors for different core diameters. For Si, As_2S_3 and CS_2 core HOFs with optimized core diameters, the lateral alignment errors are 2.48 μm, 2.36 μm, and 2.44 μm for 1 dB additional loss, respectively, and 4.37 μm, 4.12 μm, and 4.31 μm for 3 dB additional loss, respectively. These are comparable with the offset errors of the traditional SMF, 2.50 μm for 1 dB and 4.32 μm for 3 dB loss, respectively. Thus the conclusion of our investigation is that the SMF alignment techniques could be well applied to these HOFs with nanospikes at the interface. It is interesting to note that the sensitivity of misalignment declines when the core diameter is smaller than the optimized core diameter. We found the slopes of blue curves in Fig. 8 rise more slowly compared with other curves. This is because the mode area increases with decreasing core diameter. And as the mode area becomes larger, it tends to be less sensitive to lateral misalignment, although the mode mismatch increases. When the lateral offset increases to several micrometers, the coupling loss of smaller core is even less than that of the optimized condition. For example, the slope of the As_2S_3 HOF with 0.22 μm core diameter as a function of the alignment error are more gentle compared with that of the 0.24 μm core HOF. When the lateral alignment error is larger than 3 μm, the coupling loss of the As_2S_3 HOF with a core diameter of 0.22 μm is even smaller than that of the optimized-core HOF with the same lateral alignment error.

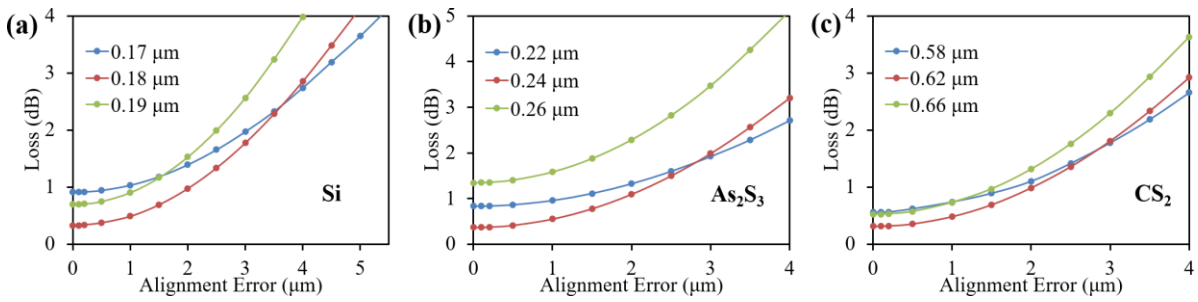

Fig. 8. The coupling loss of (a) Si, (b) As_2S_3 and (c) CS_2 core HOFs with different core diameters as a function of alignment errors.

This article has been accepted for publication in a future issue of this journal, but has not been fully edited. Content may change prior to final publication. Citation information: DOI 10.1109/JPHOT.2018.2856506, IEEE Photonics Journal

5. Interface and endface reflectivity

At the fiber endface, Fresnel reflection will contribute to the coupling loss and the specific reflection properties should be considered in many applications, for example in coupling between laser diodes and fibers. Endface reflection properties of subwavelength-core HOFs are distinctly different from traditional SMFs. When the core diameter is on the order of the wavelength scale, the primary contribution to the endface reflection is from the high index core, resulting in a high reflection loss. For example, the Fresnel reflection of the HOFs-air interface will be close to the bulk core material-air interface reflectivity, which is 30.6%, 17.5%, and 5.2%, respectively, for Si, As_2S_3 and CS_2 core HOFs. However, when the core is in the subwavelength scale, the reflectivity of the HOFs strongly depends on the core diameter. Although it has been reported that the nanospike could reduce the Fresnel reflection at the HOF interface to a value approaching that of the silica cladding, the detailed optimization and analysis has not yet been investigated.

When optimized, the interface Fresnel reflection between a HOF nanospike and a SMF could actually approach zero, and thus be ignored when mode-matching is made. For instance, as shown in Fig. 9 (a), the interface reflectivity between the Si-core HOF and the SMF calculated by Equation (6), is less than 10^{-7} when the core size is 0.18 μm. However, an air-interface is sometimes inevitable in operation. As mentioned above, the mechanical splicing technique is an effective and robust way to couple light between a subwavelength core HOF and a SMF, especially suitable for liquid and soft-glass cores that have low melting points. When using this method, an air interface may occur between the two fibers during connecting [55]. Thus the air-HOF interface reflectivity has also been calculated via Equation (6), as shown in Fig. 4(b). Note, the accuracy of this model was confirmed by calculating the endface reflectivity of silica nanofibers, which agrees well with Wang et al. [56]. The Fresnel reflection at the air interface decreases with decreasing core diameters. A higher refractive index of the core material generally results in a larger endface Fresnel reflectivity. However, when the core diameter is optimized on a subwavelength scale, the reflectivity approaches 3.4% for all three types of HOFs, which is close to Fresnel reflectivity of bulk silica at air interface. When mechanically splicing the liquid-core HOFs, the interface will most likely be liquid, not air, to avoid evaporation [54]. Contrast to the air-HOF interface, the reflectivity of the liquid-HOF interface is slightly increased when the core diameter decreases. The interface reflectivity increases from 0.07% to 0.21% when the liquid-core diameter changes from 1.00 μm to 0.56 μm. This is because the smaller the liquid-core, the larger the difference between the effective index of the liquid-core HOF and the liquid. However, the reflectivity is still much smaller compare to that at the air-interface. It is interesting to note that another type of the nanospike, a fused silica nanospike, can be utilized to reduce the Fresnel back-reflection to negligible level [57], which is also very useful for all-fiber optofluidic applications [57, 58].

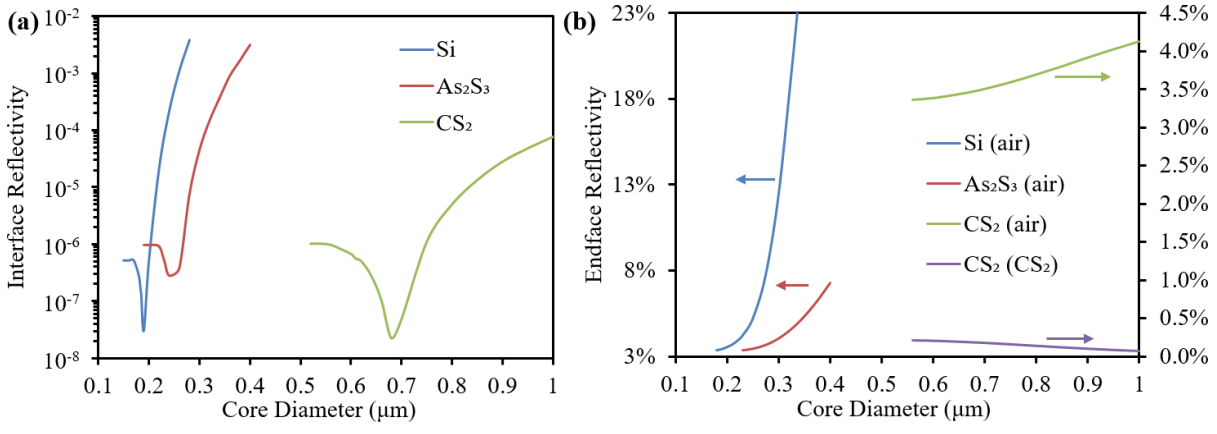

Fig. 9. (a) The interface reflectivity between an optimized HOF nanospike and SMF28. (b) The endface reflectivity of the HOF nanospike to air.

5. Conclusions

We have proposed an all-fiber integration strategy for small-core HOFs incorporating high index materials such as Si, As_2S_3 and CS_2 based on a tapered subwavelength-core approach. The effects of the MFD, mode shape, effective refractive index, tapering beat length, interface and endface reflections are all considered, and the optimized parameters such as subwavelength core diameter, single mode condition as well as the transition length have been explored. Furthermore, the core fabrication errors and misalignment tolerances have been discussed in detail. The fabrication tolerance of the subwavelength core is critical for the interface coupling loss, for example, the tolerance for the Si core HOF is only ±0.01 μm for 1dB loss. Considering the required taper transition length, a positive error (i.e., larger core size) would be recommended. The lateral offset tolerance of the optimized subwavelength-core HOFs is comparable to that of SMFs, indicating that standard commercial connection techniques developed for SMFs could be applied to the HOFs structures. The optimized parameters and detailed analysis of the coupling loss of HOFs will benefit all-fiber integration of HOFs and promote their application in wide-ranging areas.

Acknowledgements

This work was supported in part by the National Natural Science Foundation of China (grants 61475119 and 61775041), in part by the Shanghai Pujiang Program (17PJ1400600) and in part by the National Key R&D Program of China (2016YFC0201401)

References

[1] W. L. Barnes, A. Dereux and T. W. Ebbesen, "Surface plasmon subwavelength optics," Nature, vol. 424, no. 6950, pp. 824-30, 2003.
[2] V. G. Ta'eed, N. J. Baker, L. Fu, K. Finsterbusch, M. R. Lamont, D. J. Moss, H. C. Nguyen, B. J. Eggleton, D. Y. Choi, S. Madden, and B. Luther-Davies, "Ultrafast all-optical chalcogenide glass photonic circuits," Opt. Express, vol. 15, no. 15, pp. 9205-21, 2007.
[3] M. Dragoman, and D. Dragoman, "Plasmonics: Applications to nanoscale terahertz and optical devices", Progr. Quant. Electr., vol. 32, no. 1, pp. 1-41, 2008.
[4] V. R. Almeida, R. R. Panepucci and M. Lipson, "Nanotaper for compact mode conversion," Opt. Lett., vol. 28, no. 15, pp. 1302-4, 2003.
[5] Y. Kanamori, M. Sasaki and K. Hane, "Broadband antireflection gratings fabricated upon silicon substrates," Opt. Lett., vol. 24, no. 20, pp. 1422-4, 1999.
[6] Z. Cheng and H. K. Tsang, "Experimental demonstration of polarization-insensitive air-cladding grating couplers for silicon-on-insulator waveguides," Opt. Lett., vol. 39, no. 7, pp. 2206-9, 2014.
[7] J. M. Lee, K. J. Kim and G. Kim, "Enhancing alignment tolerance of silicon waveguide by using a wide grating coupler," Opt. Express, vol. 16, no. 17, pp. 13024-31, 2008.
[8] D. Taillaert, F. Van Laere, M. Ayre, W. Bogaerts, D. Van Thourhout, P. Bienstman, and R. Baets, "Grating couplers for coupling between optical fibers and nanophotonic waveguides," Japan. J. Appl. Phys., vol. 45, no. 8A, pp. 6071-7, 2006.
[9] L. Tong, R. R. Gattass, J. B. Ashcomv, S. L. He, J. Y. Lou, M. Y. Shen, I. Maxwell, and E. Mazur, "Subwavelength-diameter silica wires for low-loss optical wave guiding," Nature, vol. 426, pp. 816-9, 2003.
[10] X. Wu and L. Tong, "Optical microfibers and nanofibers," Nanophotonics, vol.2, no. 5-6, pp. 407-28. 2013.
[11] X. S. Jiang, Y. Chen, G. Vienne, and L. Tong, "All-fiber add-drop filters based on microfiber knot resonators," Opt. Lett., vol. 32, no. 12, pp. 1710-2, 2007.
[12] M. Sumetsky, Y. Dulashko, J. M. Fini, A. Hale, and D. J. DiGiovanni, "The Microfiber Loop Resonator: Theory, Experiment, and Application," J. Lightwave Technol., vol. 24, no. 1, pp. 242-50, 2006.
[13] L. Xiao and T. A. Birks, "High finesse microfiber knot resonators made from double-ended tapered fibers," Opt. Lett., vol. 36, no. 7, pp. 1098-100, 2011.
[14] M. C. Frawley, I. Gusachenko, V. G. Truong, M. Sergides, and S. Nic Chormaic, "Selective particle trapping and optical binding in the evanescent field of an optical nanofiber," Opt. Express, vol. 22, no. 13, pp. 16322-34, 2014.
[15] W. J. Wadsworth, A. Ortigosa-Blanch, J. C. Knight, T. A. Birks, T. Man, and P. S. Russell, "Supercontinuum generation in photonic crystal fibers and optical fiber tapers: a novel light source," J. Opt. Soc. Am. B, vol. 19, no. 9, pp. 2148-55, 2002.
[16] R. Zhang, J. Teipel and H. Giessen, "Theoretical design of a liquid-core photonic crystal fiber for supercontinuum generation," Opt. Express, vol. 14, no. 15, pp. 6800-12, 2006.
[17] J. M. Dudley, G. Genty and S. Coen, "Supercontinuum generation in photonic crystal fiber," Rev. Mod. Phys., vol. 78, no. 4, pp. 1135-84, 2006.
[18] N. Granzow, M. A. Schmidt, W. Chang, L. Wang, Q. Coulombier, J. Troles, P. Toupin, I. Hartl, K. F. Lee, M. E. Fermann, L. Wondraczek, and P. S. Russell, "Mid-infrared supercontinuum generation in As_2S_3-silica "nano-spike" step-index waveguide," Opt. Express, vol. 21, no. 9, pp. 10969-77, 2013.
[19] W. Gao, M. El Amraoui, M. Liao, H. Kawashima, Z. Duan, D. Deng, T. Cheng, T. Suzuki, Y. Messaddeq, and Y. Ohishi, "Mid-infrared supercontinuum generation in a suspended-core As_2S_3 chalcogenide microstructured optical fiber," Opt. Express, vol. 21, no. 8, pp. 9573-83, 2013.
[20] Y. Xu, X. Chen and Y. Zhu, "Modeling of micro-diameter-scale liquid core optical fiber filled with various liquids," Opt. Express, vol. 16, no. 12, pp. 9205-12, 2008.
[21] M. Alexander Schmidt, A. Argyros and F. Sorin, "Hybrid Optical Fibers– An Innovative Platform for In- Fiber Photonic Devices," Adv. Opt. Mater., vol. 4, no. 1, pp. 13-36, 2016.
[22] C. Markos, J. C. Travers, A. Abdolvand, B. J. Eggleton, and O. Bang, "Hybrid photonic-crystal fiber," Rev. Mod. Phys., vol. 89, no. 4, pp. 045003, 2017.

[23] J. Ballato, T. Hawkins, P. Foy, B. Yazgan-Kokuoz, C. McMillen, L. Burka, S. Morris, R. Stolen, and R. Rice, "Advancements in semiconductor core optical fiber," Opt. Fiber Technol., vol. 16, no. 6, pp. 399-408, 2010.
[24] J. Ballato, T. Hawkins, P. Foy, R. Stolen, B. Kokuoz, M. Ellison, C. McMillen, J. Reppert, A. M. Rao, M. Daw, S. Sharma, R. Shori, O. Stafsudd, R. R. Rice, and D. R. Powers, "Silicon optical fiber," Opt. Express, vol. 16, no. 23, pp. 18675-83, 2008.
[25] K. Kieu, L. Schneebeli, R. A. Norwood, and N. Peyghambarian, "Integrated liquid-core optical fibers for ultra-efficient nonlinear liquid photonics," Opt. Express, vol. 20, no. 7, pp. 8148-54, 2012.
[26] Y. Zhu, X. Chen, Y. Xu, and Y. Xia, "Propagation Properties of Single-Mode Liquid-Core Optical Fibers with Subwavelength Diameter," J. Lightwave Technol., vol. 25, no. 10, pp. 3051-6, 2007.
[27] M. Chemnitz, M. Gebhardt, C. Gaida, F. Stutzki, J. Kobelke, J. Limpert, A. Tünnermann and M. A. Schmidt, "Hybrid soliton dynamics in liquid-core fibres," Nat. Commun., vol. 8, no. 42, pp. 1-11, 2017.
[28] D. Churin, T. N. Nguyen, K. Kieu, R. A. Norwood, and N. Peyghambarian, "Mid-IR supercontinuum generation in an integrated liquid-core optical fiber filled with CS_2," Opt. Mater. Express, vol. 3, no. 9, pp. 1358-64, 2013.
[29] N. Granzow, S. P. Stark, M. A. Schmidt, A. S. Tverjanovich, L. Wondraczek, and P. S. Russell, "Supercontinuum generation in chalcogenide-silica step-index fibers," Opt. Express, vol. 19, no. 21, pp. 21003-10, 2011.
[30] P. Mehta, N. Healy, T. D. Day, J. R. Sparks, P. J. Sazio, J. V. Badding, and A. C. Peacock, "All-optical modulation using two-photon absorption in silicon core optical fibers," Opt. Express, vol. 19, no. 20, pp. 19078-83, 2011.
[31] F. H. Suhailin, N. Healy, Y. Franz, M. Sumetsky, J. Ballato, A. N. Dibbs, U. J. Gibson, and A. C. Peacock, "Kerr nonlinear switching in a hybrid silica-silicon microspherical resonator," Opt. Express, vol. 23, no. 13, pp. 17263-8, 2015.
[32] A. C. Peacock, J. R. Sparks and N. Healy, "Semiconductor optical fibres: progress and opportunities," Laser & Photonics Rev., vol. 8, no. 1, pp. 53-72, 2014.
[33] A. F. Abouraddy, M. Bayindir, G. Benoit, S. D. Hart, K. Kuriki, N. Orf, O. Shapira, F. Sorin, B. Temelkuran, and Y. Fink, "Towards multimaterial multifunctional fibres that see, hear, sense and communicate," Nat. Mater., vol. 6, no. 5, pp. 336-47, 2007.
[34] B. L. Scott, K. Wang and G. Pickrell, "Fabrication of n-Type Silicon Optical Fibers," IEEE Photon. Tech. Lett., vol. 21, no. 24, pp. 1798-800, 2009.
[35] C. Hou, X. Jia, L. Wei, S. Tan, X. Zhao, J. D. Joannopoulos, and Y. Fink, "Crystalline silicon core fibres from aluminium core preforms," Nat. Commun., vol. 6, no. 6248, pp. 1-6, 2015.
[36] L. Xiao, T. A. Birks and W. H. Loh, "Hydrophobic photonic crystal fibers," Opt. Lett., vol. 36, no. 23, pp. 4662-4, 2011.
[37] H. W. Lee, M. A. Schmidt, R. F. Russell, N. Y. Joly, H. K. Tyagi, P. Uebel, and P. S. Russell, "Pressure-assisted melt-filling and optical characterization of Au nano-wires in microstructured fibers," Opt. Express, vol. 19, no. 13, pp. 12180-9, 2011.
[38] N. Healy, J. R. Sparks, P. J. Sazio, J. V. Badding, and A. C. Peacock, "Tapered silicon optical fibers," Opt. Express, vol. 18, no. 8, pp. 7596-601, 2010.
[39] A. C. Peacock, U. J. Gibson and J. Ballato, "Silicon optical fibres - past, present, and future," Advances in Physics: X, vol. 1, no. 1, pp. 114-27, 2016.
[40] S. Xie, F. Tani, J. C. Travers, P. Uebel, C. Caillaud, J. Troles, M. A. Schmidt, and P. S. Russell, "As2S3-silica double-nanospike waveguide for mid-infrared supercontinuum generation," Opt. Lett., vol. 39, no. 17, pp. 5216-9, 2014.
[41] H. Ren, O. Aktas, Y. Franz, A. F. J. Runge, T. Hawkins, J. Ballato, U. J. Gibson, and A. C. Peacock, "Tapered silicon core fibers with nano-spikes for optical coupling via spliced silica fibers," Opt. Express, vol. 25, no. 20, pp. 24157-63, 2017.
[42] K. Z. Aghaie, M. J. F. Digonnet, and S. Fan, "Optimization of the splice loss between photonic-bandgap fibers and conventional single-mode fibers," Opt. Lett., vol. 35, no. 12, pp. 1938-40, 2010.
[43] S. Gao, Y. Wang, C. Tian, and P. Wang, "Splice Loss Optimization of a Photonic Bandgap Fiber via a High V-Number Fiber," IEEE Photonic. Tech. L., vol. 26, no. 21, pp. 2134-7, 2014.
[44] L. Xiao, M. S. Demokan, W. Jin, Y. Wang, and C. Zhao, "Fusion splicing photonic crystal fibers and conventional single-mode fibers: Microhole collapse effect," J. Lightwave Technol., vol. 25, no. 11, pp. 3563-74, 2007
[45] C. R. Pollack, Fundamentals of Optoelectronics. Irwin, Chicago, 1995.
[46] M. Artiglia, G. Coppa, P. Divita, M. Potenza, and A. Sharma, "Mode field diameter measurements in single-mode optical fibers," J. Lightwave Technol., vol. 7, pp. 1139-52, 1989.
[47] S. Kedenburg, M. Vieweg, T. Gissibl, and H. Giessen, "Linear refractive index and absorption measurements of nonlinear optical liquids in the visible and near-infrared spectral region," Opt. Mater. Express, vol. 2, no. 11, pp. 1588-611, 2012.
[48] P. Klocek, Handbook of infrared optical materials. New York: Marcel Dekker, 1991.
[49] W. S. Rodney, I. H. Malitson and T. A. King, "Refractive index of arsenic trisulfide," J. Opt. Soc. Am., vol. 48, no. 9, pp. 633 - 5, 1958.
[50] N. Kejalakshmy, A. Agrawal, Y. Aden, D. M. H. Leung, B. M. A. Rahman, and K. T. V. Grattan, "Characterization of silicon nanowire by use of full-vectorial finite element method," Appl. Opt., vol. 49, no. 16, pp. 3173-81, 2010.
[51] A. W. Snyder, and J. D. Love, Optical waveguide theory. Chapman and Hall, New York, 1983.
[52] A. Hartung, S. Brueckner and H. Bartelt, "Limits of light guidance in optical nanofibers," Opt. Express, vol. 18, no. 4, pp. 3754-61, 2010.
[53] D. Marcuse, "Loss Analysis of Single-Mode Fiber Splices," Bell Syst. Tech. J., vol. 56, no. 5, pp. 703-18, 1977.
[54] L. Xiao, N. V. Wheeler, N. Healy, and A. C. Peacock, "Integrated hollow-core fibers for nonlinear optofluidic applications," Opt. Express, vol. 21, no. 23, pp.28751-7, 2013.
[55] K. Kieu, L. Schneebeli, R. A. Norwood, and N. Peyghambarian, "Integrated liquid-core optical fibers for ultra-efficient nonlinear liquid photonics," Opt. Express, vol. 20, no. 7, pp. 8148-54, 2012.
[56] S. Wang, Z. Hu, H. Yu, W. Fang, M. Qiu, and L. Tong, "Endface reflectivities of optical nanowires," Opt. Express, vol. 17, no. 13, pp. 10881-6, 2009.
[57] R. Zeltner, S. Xie, R. Pennetta and P. S. Russell, "Broadband, lensless, and optomechanically stabilized coupling into microfluidic hollow-core photonic crystal fiber using glass nanospike," ACS Photon., vol. 4, no. 2, pp. 378-83, 2017.
[58] Y. Hao, L. Xiao and F. Benabid, "Optimized design of unsymmetrical gap nodeless hollow core fibers for optofluidic applications," J. Lightwave Technol., vol. 36, no. 16, pp. 3162-8, 2018.